Asian Journal of Physical and Chemical Sciences

3(1): 1-10, 2017; Article no.AJOPACS.35916
ISSN: 2456-7779

Spectral, Optical, Mechanical and Thermal Studies of a New NLO Material

G. Indramahalakshmi[1*]

[1]Faculty of Chemistry, Cardamom Planters Association College, Bodinayakanur – 625513, India.

Author's contribution

The sole author designed, analyzed and interpreted and prepared the manuscript.

Article Information

DOI: 10.9734/AJOPACS/2017/35916
Editor(s):
(1) A. Venkataramana, Department of Chemistry, Department of Materials Sci., Dean Faculty of Science & Technology, Gulbarga University, Kalaburagi, India.
Reviewers:
(1) A. Ayeshamariam, Khadir Mohideen College, India.
(2) K. Rajesh, AMET University, India.
Complete Peer review History: http://www.sciencedomain.org/review-history/20646

Original Research Article

Received 2nd August 2017
Accepted 20th August 2017
Published 24th August 2017

ABSTRACT

A new NLO crystal, glycinium *para*-toluenesulfonate (GPTS) is synthesized. The FT-IR study substantiated the formation of anion and cation by proton shift from *para*-toluenesulfonic acid (PTSA) to glycine resulting in adduct formation. Meyer's index shows that GPTS belongs to soft category material. Vibrations due to all functional groups appeared in their respective regions confirming adduct formation. The presence of anion and cation is confirmed by ^{1}H-NMR spectra. All the signals in ^{13}C NMR spectrum correlate very well with the proposed structure with 1:1 molecular formula ratio. TGA/DTA analysis deduced the absence of water, presence of weak hydrogen bonding, higher melting point than PTSA and 1:1 molecular formula ratio. UV–Vis-DRS transmission studies show that the grown crystal has 80% optical transparency. The cut-off wavelength and band gap energy were found to be 265 nm and 4.22 eV respectively. The emission spectrum indicates that the sample exhibits green lighting emission sharply at 532 nm and it will be useful for fabricating green light emitting diodes. SHG efficiency is 1.5 times that of KDP. Thus the new material qualifies itself for possible use as NLO applications.

Keywords: NLO material; Tauc graph; SHG; Meyer's index; amino acid; TGA/DTA.

**Corresponding author: E-mail: ayyan1960@gmail.com;*

1. INTRODUCTION

Organic materials have attracted much attention due to their potential applications in optical data storage, color displays, optical communications, efficient Raman lasers and second harmonic generators [1-5] and nonlinear optical materials (NLO) [6-14]. The organic-organic materials show high nonlinearity and flexibility. They have higher resistance to optical damage and can be used in frequency doubling and laser fusion experiments [15]. Due to the absence of conjugated bonds, aminoacids exhibit strong transparency in the UV visible spectral regions. The presence of hydrogen bonds and zwitter ionic nature of the molecule favours crystal hardness [16]. The main steering force of such molecular solids is the hydrogen bonding that decides the application of these materials. Studies on crystalline salts of amino acids and their derivatives are of greater attention since they show good NLO activities. Glycine is known to form adducts with benzoyl, picric acid and meta-nitrobenzoic acid [17-19]. PTSA has been reported to form adduct with betaine, L-histidine, L-alaninium and L-valinium [20-23]. The single crystal structure of PTSA with Glycine alone is reported [24]. So, the aim of the present work is to synthesize the crystal and characterize its spectral, optical, mechanical and thermal studies of the NLO material.

2. EXPERIMENTAL

The synthesis of the adduct glycinium para-toluenesulfonate (GPTS) was carried out by mixing 0.5M PTSA and 0.5M glycine aqueous solutions in 1:1 stoichiometric ratio. The solution was heated with stirring for few minutes to get homogenous solution and then filtered. Slow evaporation of the hot filtered solution at room temperature yielded large colorless crystals within five days. Elemental analysis was carried out in Elemental Vario EL III Germany. The ^{1}H NMR and ^{13}C NMR spectras were recorded in Bruker DPX 400 instrument using D_2O. The IR spectra was recorded as KBr pellets using JASCO 640 Plus Spectrometers. The absorbance spectra was recorded as KBr pellet using a JASCO 530V UV-Visible Spectrophotometer. Reflectance was measured using JASCO UV-VIS-DRS V-750 spectrophotometer. The thermogram was recorded on a Netzsch STA 409 simultaneous thermal analyzer. Mechanical properties were analysed by Vicker's micro hardness tester Shimadzu-HMV-2. Q-switched mode locked Nd: YAG laser (λ = 1064 nm) was used to assess the NLO behavior of the compound.

3. RESULTS AND DISCUSSION

The calculated/ observed values of elements present are C= 46.75/ 47.00, H= 5.62/ 5.01, N= 6.06/ 6.45, S= 13.85/ 13.30, O= 27.70/ 27.02%. Thus the compound has 1:1 molecular formula ratio. The compound is soluble in coordinating solvents like water, DMSO, MeOH and has the possible structure.

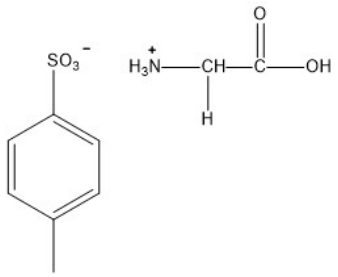

3.1 Solubility Studies

Solubility of GPTS was studied in double distilled water. Saturated solution was prepared at various temperatures (30, 35, 40, 45°C) with the help of a constant temperature bath and the amount of solute dissolved was measured gravimetrically [25]. Fig. 1 shows the increase in solubility with temperature rise, exhibiting a high solubility coefficient. Photograph of single crystals of GPTS obtained are shown in Fig. 2.

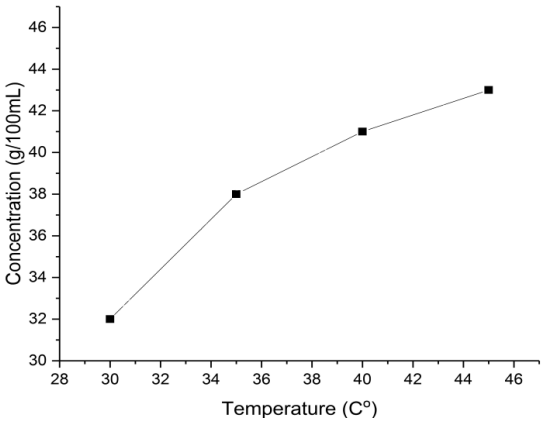

Fig. 1. Solubility curve of GPTS

3.2 Micro Hardness Measurements

Micro hardness testing is one of the best methods for understanding the mechanical

properties of materials. Hardness of the material is a measure of resistance, that offers to deformation [26]. The indentations were made on the flat surface by varying the load from 25 to 100 g using Shimadzu-HMV-2 fitted with Vicker's pyramidal indenter. The indentation time was kept as 10 seconds for all the loads. The Vickers's hardness number H_v was calculated from the following expression, $H_v = (1.8544\ P)/d^2$ kg/mm^2 where P is the applied load in kg and d is the diagonal length of the indentation impression. A plot obtained between the hardness number and the load is shown in Fig. 3. The relation connecting the applied load and diagonal length'd' of the indentor in micrometer is given by Meyer's law $P = ad^n$, where n is the Meyer's index or work hardening coefficient [27]. A plot obtained between log (P) and log (d) gives a straight line Fig. 4. Slope of straight line is Meyer's index. From many observations on various materials Onitsch pointed out that 'n' lies between 1 and 1.6 for moderately hard materials, and it is more than 1.6 for soft materials, The observed value of Meyer's index for GPTS is 4.1 and hence GPTS belongs to the soft materials category.

Fig. 2. Photograph of GPTS crystal

3.3 Thermal Analysis

The thermograms are shown in Fig. 5 and the analysed data are provided in Table 1. There was no weight loss observed around 100ºC indicating the absence of water in the sample, that are thermally stable up to 191ºC. Below decomposition temperature, there was no detectable weight loss and hence the crystals have rejected solvent molecules during crystallization which is unusual for PTSA.

Degradation took place above the decomposition temperature in different stages. Melting point of glycine is 250ºC. The endothermic peak inflexion point at 191ºC in DTA correspond to the melting point of GPTS. This melting point is close to the average m.pt.(250+103/2) showing the formation of 1:1 adduct. This value higher than that of PTSA (103ºC) is due to the utilization of thermal energy to overcome the valence bonding between the glycinium cation and the *para*-toluenesulphonate anion, which happens during the initial stage of decomposition.

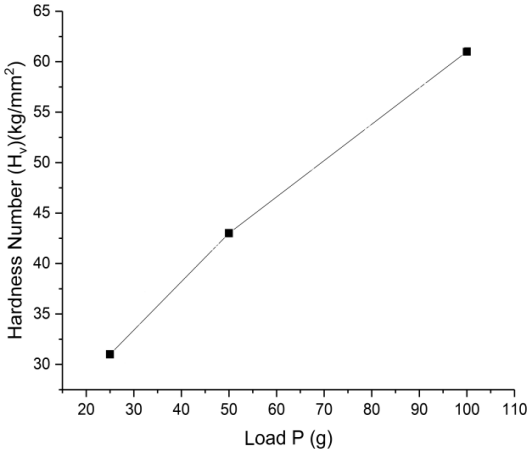

Fig. 3. Plot of Vicker's hardness for GPTS

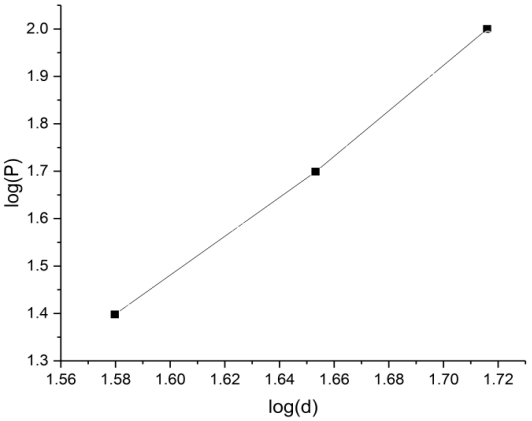

Fig. 4. Log P versus log d

During next stage, a sudden decomposition took place at a stretch, between 230-360ºC with a weight loss of 72% due to the expulsion of SO_3, CO_2 and H_2O [28], the corresponding peak in DTA curve occurring at 274.1ºC. The reaction of simplest amino acid on heating, include the condensation reaction of carbonyl and amino group leading to the formation of peptide bonds with liberation of water [9,12]. In the dehydration,

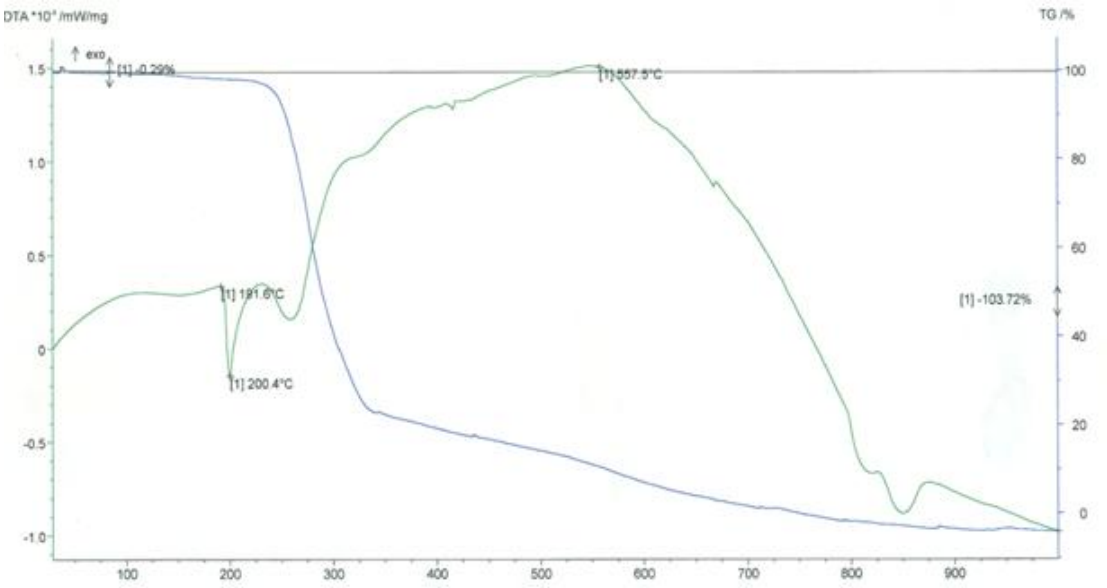

Fig. 5. TGA/DTA curves for GPTS

Table 1. Thermal data for GPTS

Temperature range °C	Inflexion point °C	%weight loss	Endo/ Exothermic	Liberation process
125-230	191	0	Endo	Melting point
230-360	274	72	Endo	(decomposition of PTSA) CO_2, SO_3, H_2O
360-800 (includes 5 stages in DTA)	305, 385,475, 525, 555	28	Exo	H_2O, CO, NH_3

at the first stage, water molecule is not liberated immediately, instead it is absorbed by alumina, which acts as a catalyst and is then released along with remaining fragments of glycine (CO and NH_3) at 590ºC above 360ºC. Because of this, an endothermic effect is noted in the DTA. A mass loss of 28% above 360ºC is due to the release of H_2O, CO, NH_3 [9,12].

From TGA/DTA it is proved that;

1. Water is absent in the compound.
2. Hydrogen bonding is present.
3. Compound has higher melting point than PTSA.
4. Adduct molecular formula ratio is 1:1

3.4 IR Spectrum Analysis

The infrared spectrum of the compound is presented in Fig. 6 and the vibrational frequencies are given in Table 2. A band in the range 2925 cm^{-1} can be assigned to the stretching vibration of the (CH_3) group. The band around 1395 cm^{-1} is due to the symmetric deformation of methyl group. The peaks due to ν(C=C)ϕ, 1619 and 1505 cm^{-1} show the presence of benzenoid ring. A strong band observed at 1123 cm^{-1} (βCHϕ) coincides well with the literature values observed in the range 1220-1120 cm^{-1} [29] and is considered to be a measure of the degree of delocalization of electrons due to hydrogen bonding with the oxygen atoms in the SO_3^- group and thus it is a characteristic peak of PTSA in the adduct. The three bands appearing at 822, 860 and 956 cm^{-1} are attributed to out of plane (C-H) bending vibrations ascribed to the *para* substituted aromatic rings [30]. A very strong band at 799 cm^{-1} is assigned to the ring breathing mode in agreement with that (800 cm^{-1}) for a number of *para*-substituted benzene derivatives [29]. It is well documented that sulfonic acids have a strong, broad and split bands in the region of

1000 - 1250 cm^{-1} [29,31]. The mode at 1036 cm^{-1} can be assigned to SO_3^- group of the PTSA as reported in [32], confirming presence of PTSA in the adduct.

The presence of strong and broad peaks above 3100 cm^{-1} shows the presence of glycine as glycinium cation rather than zwitter ion (COO^- and NH_3^+). The broad, strong absorption in the region 3233-2364 cm^{-1} for the title compound is in good agreement with the literature data [33], that salts of primary amino acids are characterised by broad and strong absorption in the region of 3333-2380 cm^{-1} resulting from superimposed OH, CH, CH_2, CH_3 and NH_3^+ stretching bands along with H-bonding of the type N – H - - - O. Thus the nature and presence of COOH and NH_3^+ groups are confirmed.

A very strong band at 1756 cm^{-1}, assigned to υC=O is higher than that the stretching vibration frequency of COO^- ion as mentioned in earlier studies [34] showing the presence of COOH group. A little decrease in this value from that of free COOH (1800 cm^{-1}) may be due to the intermolecular H-bonding C=O. . .H – N. When COOH forms H- bonding, it results in a broad band centred at 3100-2900 cm^{-1} that superimposes on υCH bands. A broad band at 3442 cm^{-1} is assigned to υOH. These facts justify the proposed structure with H-bondings. All other vibrations due to all functional groups appeared in their respective regions confirming adduct formation.

3.5 NMR Spectral Analysis

The ^1H NMR spectrum is presented in Fig. 7 and data are presented in Table 3. The aromatic protons of phenyl ring occur in the range of 7.15 to 7.65 ppm. The protons of CH_3 group of PTSA appear as singlet at 2.32 ppm integrating for 3 protons. The singlet peak at 5.2 ppm corresponds to proton of COOH group. While the CH_2 protons are seen at 3.73 ppm, signals from protonated nitrogen viz., NH_3^+ are observed at 8.15 ppm.

The ^{13}C NMR spectrum is illustrated in Fig. 8. It exhibits peaks corresponding to aliphatic methyl carbon at 20.39 ppm and methylene carbon at 39.64 ppm. The aromatic carbons (CH) appear at 127.9 and 124.9 ppm. Signals at 139 and 141.5 ppm originate from aromatic carbons attached to methyl and sulfonic acid groups respectively. The only signal at 168.3 ppm confirms the presence of carbon of COOH. All the signals correlate very well with the proposed structure.

3.6 Absorption Spectral Analysis

The absorption spectrum of GPTS (Fig. 9) shows intense bands centered at 224 and 265 nm, attributed to n-π*/π-π* transition of the C=O and π-π* transition of the benzene ring respectively. n-π* transition is due to the direct transition of an electron from a non-bonding 'n' orbital to an anti bonding π*orbital. The crystal has lower cut-off wavelength at 265 nm which is important for efficient NLO crystal [35] and less than that of glycinium nitrate a semi organic crystals [36]. There was no absorption band beyond 265 nm, which confirmed the absence of any overtones.

3.7 UV-VIS-DRS

Fig. 10 shows 80% optical transmittance of GPTS powder. Similar transmittance window in the visible region enables good optical transmission of the second harmonic frequencies of Nd: YAG laser [37]. The measured transmission (T) can be used to calculate the absorption coefficient (α) using the relation α = (2.303 $\log(^1/_T)$)/ t ;where 't' is the thickness of the

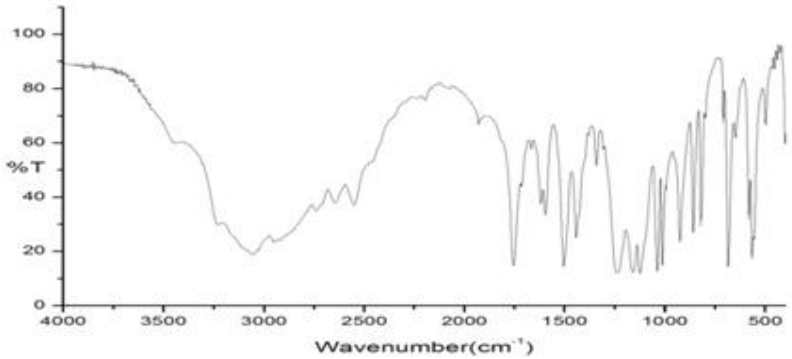

Fig. 6. FT-IR spectrum

Table 2. FT-IR Spectral assignments for GPTS

FTIR	Vibrational assignments	FTIR	Vibrational assignments
3442 m	v(OH)	1160 s	vas(SO_3), β(OH), ρt(CH_2)
3233 s	v(NH) free	1123 s	β(CH)ϕ
3061 s	vs(CH)φ	1036 s	δ(CH_3)
3021 sh	va(CH)φ	1036 s	vs(SO_3), v(C-N)
2952 s	va(CH_2)	1012 s	v(C-N)
2925 s	va(CH_3)	956 w	γ (CH)ϕ
2741 s	vs(CH_3)	927 s	ρ(CH_2)
2715sh	vs(NH_3)$^+$	860 s	γ (CH)ϕ
2646 s	vas2(NH….0)	822 s	γ (CH)ϕ
1756 s	v(C=0)	799 s	α(CCC)φ
1667 w	δa(NH_3)$^+$	711 w	γ(CCC)φ
1619 s	v(C=C)ϕ	685 s	v(C-S),γ(OH), vφskel
1596 s	vas(CC)φ	650 w	β(CCC)
1505 s	vas(CC)φ	582 s	β(OH)
1442 s	δas(CH_2)ip	566 s	δϕ(CCC),ρr(SO_3)
1414 m	v(C-C)ϕ+β(CH)ϕ, δ(CH_3)	556 s	ρr(SO_3),γφ
1395 w	δ(CH_3)	507 s	γ(OH),τ(NH_3)
1381 w	δs(CH_2)	498 w	γ(OH),τ(NH_3)
1340 m	v(C-OH)	428 w	γ(NH_3), β(C-COOH)
1307 w	β(CH)ϕ	402 m	Γskel
1232 s	v(C-CH_3), β(CH)ϕ		

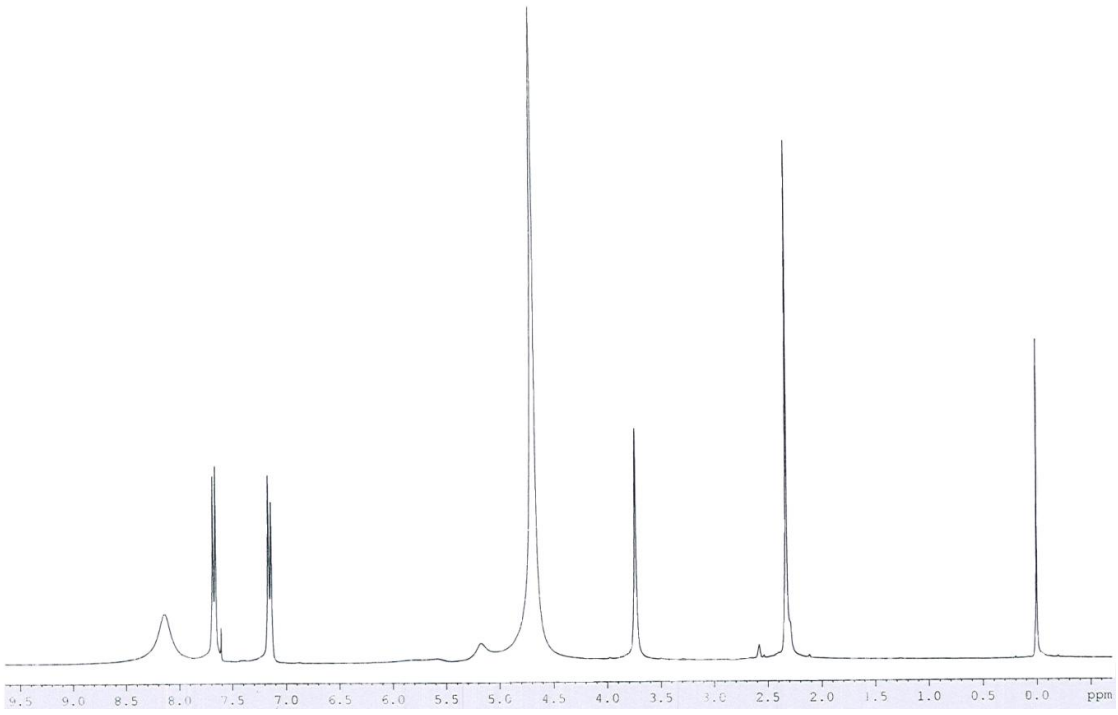

Fig. 7. ^{1}H NMR spectrum of GPTS

sample. The absorption obey the relation *(αhv)* = *A* $(E_g - hv)^{1/2}$ where *A* is a constant, E_g is the optical band gap energy. The Tauc's graph plotted between the product of absorption coefficient and the incident photon energy $(\alpha hv)^2$ with the photon energy (*hv*) shows a linear behavior that can be considered as evidence for the direct transition (Fig. 11). The wide optical

band gap energy, 4.22 eV of the crystal confirms the large transmittance in the visible region and is very close to that of L-leucinium p-toluenesulfonate monohydrate (4.26 eV) [38].

3.8 Non Linear Optical Studies

Powder SHG method is used to evaluate the bulk homogeneity of the sample. A quantitative measurement of the second harmonic generation (SHG) efficiency of GPTS was determined by the modified version of powder technique developed by Kurtz and Perry [39]. Powder GPTS was packed densely between two transparent glass slides. A high intensity Nd: YAG laser (1064 nm) with a pulse duration of 10ns, at a frequency of 10Hz was passed through the pelletized sample. The measured intensity was compared with the output intensity at 532 nm by KDP (Potassium dihydrogen phosphate) tested in a similar set up. The SHG efficiency of GPTS is approximately 1.5 times that of KDP for an input energy of 3.5 mJ/pulse. So GPTS crystal could be used for generation and mixing of frequencies over a wide range of electromagnetic spectrum including the UV and for blue green laser application [40].

Table 3. ^{1}H and ^{13}C NMR spectroscopic data in (D_2O)

^{1}H NMR		^{13}C NMR	
7.65	2H, Aro	141.5	1C, C-S
7.15	2H, Aro	139	1C, C-CH_3
2.32	3H, CH_3	127.9	2C, Aro
8.15	3H, NH_3^+	124.9	2C, Aro
5.2	1H, COOH	20.39	1C, CH_3
3.73	2H, CH_2	168.3	1C, COOH
		39.64	1C, CH_2

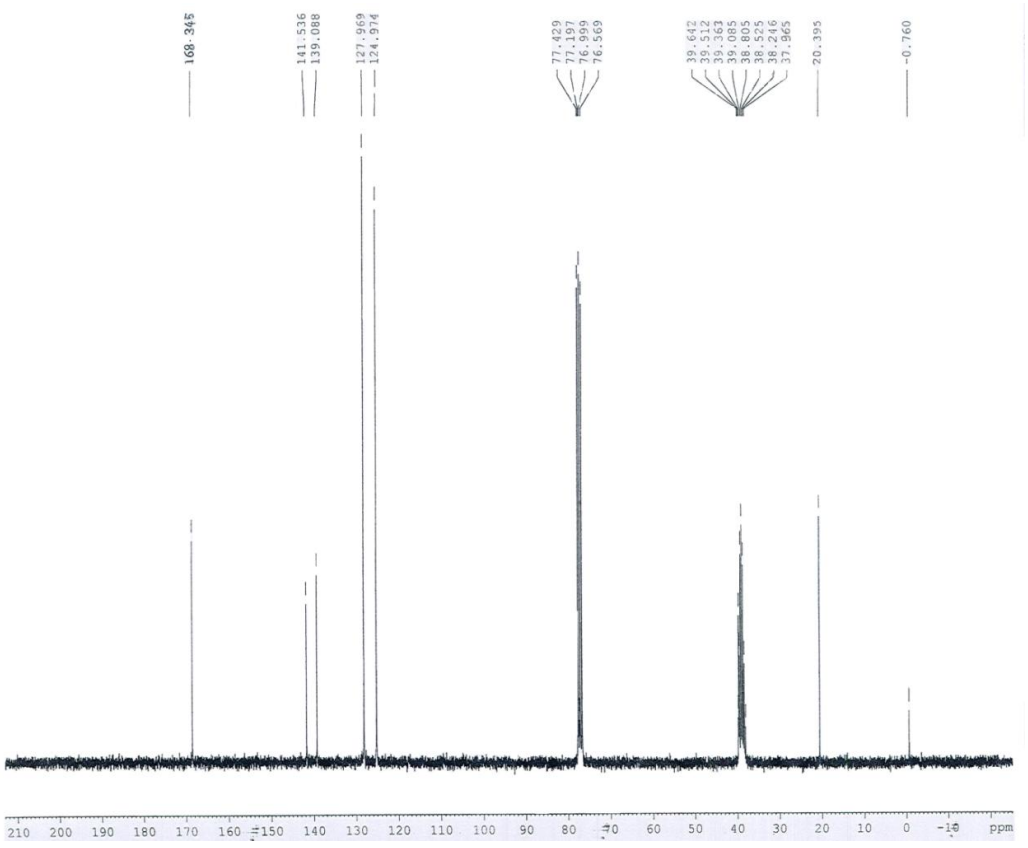

Fig. 8. ^{13}C NMR spectrum of GPTS

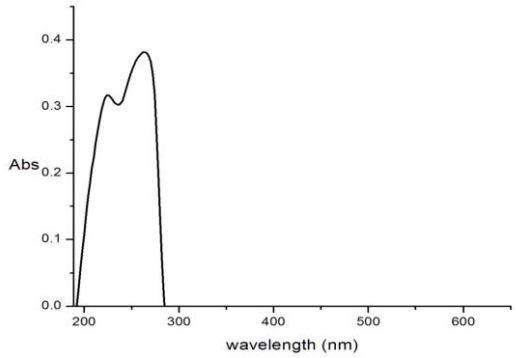

Fig. 9. UV spectrum of GPTS

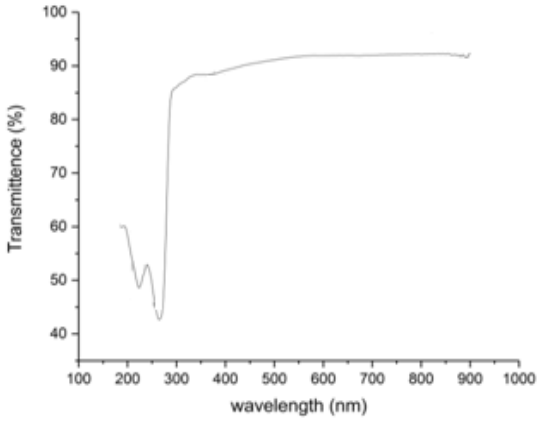

Fig. 10. UV DRS Spectrum of GPTS

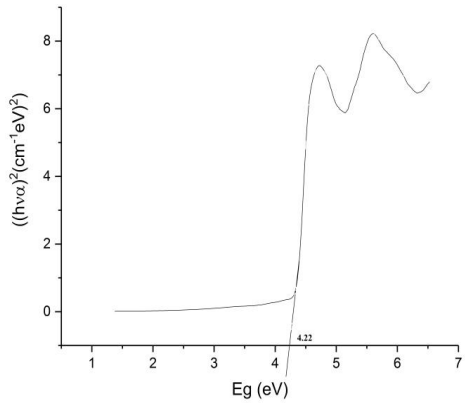

Fig. 11. Tauc Graph of GPTS

3.9 Laser Damage Threshold Study

Since high optical intensities are involved in non linear processes, laser damage threshold is an important factor for a NLO crystal to be used in a device. The study have been carried out for GPTS single crystal using a Q- Switched Nd: YAG laser (λ=1064nm) with a pulse duration of 10ns, at a frequency of 10Hz. The laser damage energy density calculated was 5.3 GW/cm^2 using the formula, Energy Density = E/A; where E is the input energy measured in millijoules and A is area of the circular spot. This value is comparable to that of L- prolinium tartrate [12].

4. CONCLUSION

NLO organic single crystal of hydrogen bonded glycinium p-toluenesulfonate (GPTS) was synthesized and grown as a single crystal by slow evaporation solution growth technique. 1:1 molecular formula ratio was obtained from elemental analysis. Infrared spectral study was used to confirm the functional groups present in the compound. The FT-IR and NMR studies substantiated the formation of anion and cation by proton shift from PTSA to glycine resulting in adduct formation. TGA/DTA analyses deduced the absence of water, presence of weak hydrogen bonding, higher melting point than PTSA and 1:1 molecular formula ratio. GPTS belongs to soft category material according to Meyer's index. The cut-off wavelength and band gap energy were found to be 265 nm and 4.22 eV respectively. The wide optical energy band gap of the grown crystal confirms that GPTS is transparent throughout the visible region. The absorption spectrum shows 80% optical transmittance in the entire region. SHG efficiency of GPTS was 1.5 times KDP. Thus the new material qualifies itself for possible use as NLO applications.

ACKNOWLEDGEMENT

Dr. G. Indramahalakshmi, thanks the management of Cardamom Planters Association College, Bodinayakanur.

COMPETING INTERESTS

Author has declared that no competing interests exist.

REFERENCES

1. Dmitriev VG, Gurzadyan GG, Nicogosyan DN. Handbook of nonlinear optical crystals. Springer-Verlag, Newyork; 1999.
2. Razze C, Ardyno M, Zanotti L, Zha M, Paorici C. Solution growth and characterisation of L-alanine single crystals. Cryst. Res. Technol. 2002;37: 456.

3. Wong MS, Bosshard C, Pan F, Gunter P. Non-classical donor–acceptor chromophores for second order nonlinear optics. Adv. Mater. 1996;8:677.
4. Marey HO, Warrn LF, Webb MS, Ebbers CA, Velsko SP, Kennedy GC, Catella GC. Second-harmonic generation in zinc tris (thiourea) sulfate. Appl. Opt. 1992;31: 5051.
5. X Q Wang, et al. Synthesis, structure and properties of a new nonlinear optical material: zinc cadmium tetrathiocyanate. *Mater. Res. Bull.* 1999;34.
6. Rajesh K, Mani A, Anandan K, Praveen Kumar P. Crystal and optical perfection, linear and nonlinear optical qualities of β alanine β alaninium picrate (βaβap) single crystal: a promising NLO crystal for optics and photonics applications. J Mater Sci: Mater Electron. 2017;28:11446-11454.
7. Rajesh K, Mani A, Praveen Kumar P. Growth and characterization of l-glycinium phosphate: A promising crystal for opto – electronics applications. Mechanics, Materials Science & Engineering. 2017;9:73-78.
DOI: 10.2412/mmse.18.52.862.
8. Pal T, Kar T, Bocelli G, Rigi L. Synthesis, growth, and characterization of l-arginine acetate crystal: A potential NLO material. Cryst. Growth Des. 2003;3:13.
9. Natarajan S, Martin Britto SA, Ramachandran E. Growth, thermal, spectroscopic, and optical studies of l-alaninium maleate, a new organic nonlinear optical material. Cryst. Growth Des. 2006;6:137.
10. Ramesh Kumar G, Gokul Raj S, Mohan R, Jeyavel R. Influence of isoelectric ph on the growth linear and nonlinear optical and dielectric properties of l-threonine single crystals. Cryst. Growth Des. 2006;6:1308.
11. Vijayan N, Ramesh Babu R, Gopalakrishnan R, Ramasamy P, Ichimura M, Palanichamy M. Growth of hippuric acid single crystals and their characterisation for NLO applications. J. Cryst. Growth. 2005;273:564.
12. Martin Britto Dhas SA, Natarajan S. Growth and characterization of L-prolinium tartrate – A new organic NLO material. Cryst. Res. Technol. 2007;42:471.
13. Haja Hameed AS, Lan CW. Nucleation, growth and characterization of L-tartaric acid-nicotinamide NLO crystals. J. Cryst. Growth. 2004;270:475.
14. Lu MK, Meng FQ, Yang ZH, Yu WT, Zeng H. Growth and characterization of urea-(DL) tartaric acid single crystals. Cryst. Res. Technol. 1996;31:834.
15. Ushashree PM, Jayavel R, Subramanian C, Ramasamy P. Growth of zinc thiourea sulfate (ZTS) single crystals: A potential semiorganic NLO material. J. Crystal Growth. 1999;197:216.
16. Delfino M. A comprehensive optical second harmonic generation study of the non-centrosymmetric character of biological structures. Mol. Cryst. Liq. Cryst. 1979;52:271-284.
17. Nagaraja HS, Upadhyaya V, Mohan P, Rao P. Sreeramana Aithal, Bhat AP. Organic nonlinear optical crystals of benzoyl glycine. J. Cryst. Growth. 1998;193:674-678.
18. Shakir M, Kushwaha SK, Maurya KK, Arora M, Bhagavannarayana G. Growth and characterization of diglycine picrate-Remarkable second-harmonic generation in centrosymmetric crystal. J. Cryst. Growth. 2009;311:3871.
19. Zheng Ji-Min, Che Yun-Xia, Wang Ru-Ji, Wang Hong-Gen. Crystal structure of 1:1 adduct of glycine and *m*-nitrobenzoic acid. Acta Phys. Chim. Sin. 1994;10(1):64.
20. Haussuhl S. Elastic and thermoelastic properties of twelve adducts of betaine, $(CH_3)_3$ NCH_2COO, with H_2O, hcl, hbr, HI, HNO_3 , H_2SO_4 , H_3PO_3 , H_3PO_4 , 1,4-toluene sulfonic acid, $mncl_2$ and kbr. Z. Kristallogr. 1989;188:311.
21. Suresh M, Asath Bahadur S, Athimoolam S. Investigations on spectroscopic, optical, thermal and dielectric properties of a new NLO material: l-Histidinium *p*-toluenesulfonate [LHPT]. Optik. 2015;126: 5452–5455.
22. Suresh M, Asath Bahadur S, Athimoolam S. Synthesis, growth and characterization of a new hydrogen bonded organic tosylate crystal: l-alaninium p-toluenesulfonate for second order nonlinear optical applications. J. Mater. Sci. Mater. Electron. 2016;27(5):4578-4589.
DOI:10.1007/s10854-016-4334-7.
23. Suresh M, Asath Bahadur S, Athimoolam S. Synthesis, growth, structural, spectral, thermal and microhardness studies of a new hydrogen bonded organic nonlinear optical material: L–valinium p–toluenesulfonate monohydrate (LVPT). J. Mol. Struct. 2016;1112:71-80.
DOI:10.1016/j.molstruc.2016.01.093.

24. Chwaleba D, Ilczyszyn M, Ciunik Z. Glycine–methanesulfonic acid (1:1) and glycine–*p*-toluenesulfonic acid (1:1) crystals: Comparison of structures, hydrogen bonds, and vibrations. J. Molecular Struct. 2007;831:119.
25. Vasudevan V, Ramesh Babu R, Ramamurthi K. Unidirectional growth of l-lysine l-lysinium dichloride nitrate (l-LLDN) single crystals by the SR method. Physica B. 2011;406:936-940.
26. Mott BW. Micro indentation hardness testing. Butterworths, London; 1956.
27. Ravindra NM, Bharadwaj RP, Sunil Kumar K, Srinivastava VK. Model based studies of some optical and electronic properties of narrow and wide gap materials. Infrared Phys. 1981;21:369.
28. Ramachandran E, Natarajan S. Crystal growth of some urinary stone constituents: I. In-vitro crystallization of L-Tyrosine and its characterization. Cryst. Res. Technol. 2002;37(11):1160.
29. Ljupco Pejov, Mirjana Ristova, Bojan Soptrajanov. Quantum chemical study of p-toluenesulfonic acid, p-toluenesulfonate anion and the water–p-toluenesulfonic acid complex. Comparison with experimental spectroscopic data. Spectrochimica Acta Part A. 2011;79:27.
30. Amalraj John, Palamari jayaprakash Yadav, Srinivasan Palaniappan. Clean synthesis of 1,8-dioxo-dodeca-hydroxanthene derivatives catalyzed by polyaniline-*p*-toluenesulfonate salt in aqueous media. J. Molecular Catalysis A: Chemical. 2006;248:121.
31. Socrates G. Infrared and Raman characteristic group frequencies, Edn -3, John Wiley & Sons: Chichester, 2001 and references therein.
32. Lorenc J, Bryndal I, Marchewka M, Sasidek W, Lis T, Hanuza J. Crystal and molecular structure of 2-aminopyridinium-4-hydroxybenzenosulfonate—IR and Raman spectra, DFT calculations and physicochemical properties. J. Raman Spectrosc. 2008;39:569.
33. Silverstein RM, Webster FX. Spectrometric identification of organic compounds. Sixth ed., John Wiley & Sons, Inc.; 1998.
34. Sundaraganesan N, Dominic Joshua B, Settu K. Vibrational spectra and assignments of 5-amino-2-chlorobenzoic acid by ab initio Hartree–Fock and density functional methods. Spectrochima Acta Part A. 2007;66:381.
35. Willard HH, Merritt LL, Dean JA, Settle FA. Instrumental methods of analysis. First Indian Edition (CBS, Delhi, 1986).
36. Martin brittodhas SA, Natarajan S. Growth and characterization of a new organic NLO material: Glycine nitrate. Optics Communications. 2007;278:434.
37. Rao CNR. Ultraviolet and visible spectroscopy of organic compound, Prentice Hall of India Pvt. Ltd., New Delhi; 1984.
38. Suresh M, Asath Bahadur S, Athimoolam S. Structural and solid state properties of L-leucinium p-toluenesulfonate mono-hydrate: An amino acid tosylate NLO crystal. J. Mater Sci Mater Electron, Aug 2016.
DOI: 10.1007/s10854-016-5572-4.
39. Kurtz SK, Perry TT. A powder technique for the evaluation of nonlinear optical materials. J. Apply. Phys. 1968;39:3798-3813.
40. Krishna Rao K, Surender V, Saritha rani B. Microhardness studies on as-grown faces of $naclo_3$ and $nabro_3$ crystals. Bull. Mater. Sci. 2002;25:641-646.

Peer-review history:
The peer review history for this paper can be accessed here:
http://sciencedomain.org/review-history/20646